RADIATION MODELING IN THE PIC-DSMC CODE PICLAS

Julian Beyer, Marcel Pfeiffer, and Stefanos Fasoulas

Institute of Space Systems, University of Stuttgart, Pfaffenwaldring 29, 70569 Stuttgart, Germany
E-mail: jbeyer@irs.uni-stuttgart.de

ABSTRACT

Atmospheric entries at high velocities can introduce considerable radiative heat fluxes. The calculation of these fluxes can be substantially impacted by different non-equilibrium effects, which are occurring in the surrounding flow. In this paper, the coupled Particle-in-Cell and Direct Simulation Monte Carlo Code PICLas is introduced and the theoretical background of the code is described. The well-established radiation solver PARADE, previously developed at IRS, is not suitable to be coupled with a DSMC code due to several reasons, which are discussed in this paper. Therefore, a new radiation solver is being developed and implemented in PICLas. Results for radiative atomic and molecular bound-bound transitions are presented and compared to the results of PARADE. Additionally, a concept for solving the radiative transfer equation using the Monte Carlo method is presented and results are shown for the classical and a noise-reducing approach.

Key words: DSMC, PICLas, Radiation, Radiation Solver, Radiative Transfer Solver.

1. INTRODUCTION

Radiative processes are important for describing and understanding plasma phenomena. The radiative heat flux can be substantial during atmospheric entries [18]. Typically, flow field simulations are conducted using conventional CFD tools, such as Navier-Stokes solvers. These solvers are well established for a wide range of flow conditions, and their efficiency in dense flow regions, where radiative heat flux becomes most important, is a particular advantage. However, treating non-equilibrium effects in the flow field, which can strongly influence the radiative heat transfer, is problematic with CFD methods. Here, gas kinetic approaches become attractive alternatives, since they are well suited for simulating non-equilibrium flows. One such approach is the Direct Simulation Monte Carlo (DSMC) method. Using this well-established approach, it is possible to compute detailed information about each flow species, including excitation temperatures, densities, and the distribution functions for each degree of freedom. Previous approaches that combine a particle code with a radiation solver [4, 19] have indeed showed promising results.

A specific case in which non-equilibrium effects are significant is the reentry of the Hayabusa capsule. Fig. 1(a) shows that the temperatures (as calculated with the DSMC code PICLas [15]) along the symmetry axis in front of the stagnation point are far from equilibrium. Although they do converge toward a single value, they cannot reach thermal equilibrium before the flow reaches the stagnation point. Figure 1(b) shows the electronic excita-

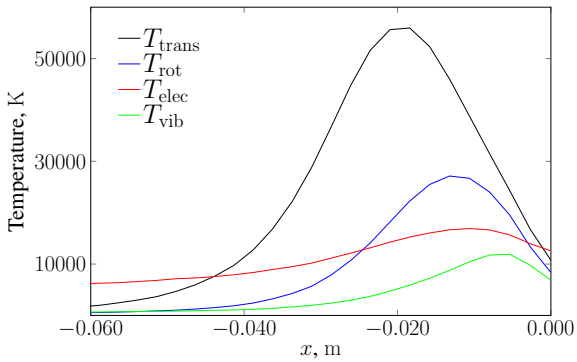

(a) Mean vibrational, rotational, electronic excitation and translational temperatures

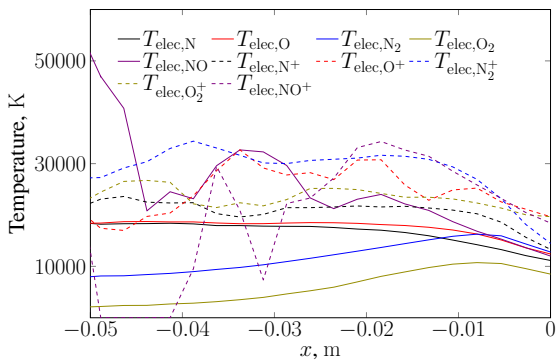

(b) Electronic excitation temperatures for different species

Figure 1: Temperatures along symmetry axis in front of stagnation point of Hayabusa reentry (h = 78.8 km, M = 40) [16].

tion temperatures of the species used in this simulation. In addition to the lack of equilibrium between the different degrees of freedom, a non-equilibrium state also exists between different species within the same degree of freedom. When calculating radiation effects, the assumption of equilibrium among all species could lead to non-negligible errors due to over- or underestimating strong radiators. Moreover, assuming a Boltzmann distribution for the excitation levels within a specific degree of freedom is also questionable in many cases.

A critical point in the radiation modeling is solving the radiative transfer equation (RTE). Here, different algorithms exist with different levels of accuracy and computational effort. With the Monte Carlo Method [8], the energy is divided into an integer number of photons whose properties, such as position, direction, and wavelength, are randomly assigned. The path of each beam through the cells is traced and the optical path is calculated. Subsequently, the RTE is solved in the direction of the beam. This method is very accurate when there are many traced photons.

This paper describes the first steps toward linking the different code structures of a flow field solver (PICLas), a radiation solver, and a radiative transfer solver, following the suggestions of Pfeiffer et al. [22]. PICLas is introduced and described in section 2.1. Initially, it was planned to use the radiation solver PARADE [24]. In a coupling context, however, PARADE has some disadvantages. These are addressed in section 2.2, where also a newly developed radiation solver for the PICLas framework is introduced. Results for atomic and molecular bound-bound radiation are shown in sections 2.2.1 and 2.2.2, respectively. Moreover, first results for solving the RTE using a Monte Carlo approach are presented in section 2.3.

2. PLASMA-GAS KINETIC AND RADIATION SOLVERS

2.1. Plasma Kinetic Code PICLas

PICLas is a coupled Particle-in-Cell (PIC) and DSMC code that enables the simulation of complex non-equilibrium chemically reacting flows, as well as plasmas in the electrostatic or electromagnetic regime [15]. Instead of solving classic continuum models like the Navier-Stokes- or the magnetohydrodynamic equations for the description of non-equilibrium plasmas, the open source code PICLas solves the Boltzmann equation

$$\left(\frac{\partial}{\partial t} + \vec{v}\frac{\partial}{\partial \vec{x}} + \frac{\vec{F}}{m}\frac{\partial}{\partial \vec{v}}\right) f = \left(\frac{\partial f}{\partial t}\right)_{\text{coll}}. \qquad (1)$$

Here, $f = f(\vec{x}, \vec{v}, t)$ is the particle distribution function at the six-dimensional phase space point $(\vec{x}, \vec{v})$ at the time t. Furthermore, m is the particle mass, $\vec{F}$ an external force

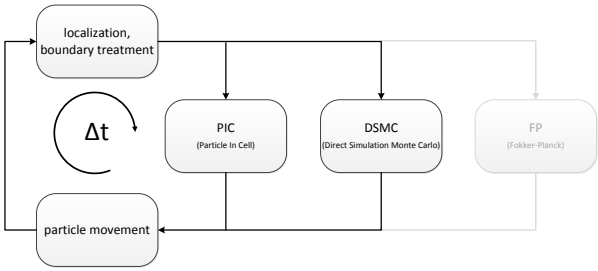

Figure 2: Typical time step of the PIC-DSMC Code PICLas, indicating the possibility to use additional solvers, e.g. a Fokker-Planck based Coulomb collision solver.

and $(\partial f/\partial t)_{coll}$ the so-called Boltzmann collision integral, which describes intermolecular collisions between the particles in the flow. The basic idea of the DSMC and PIC method is the approximation of the distribution function by a certain number of particles N at the positions $\vec{x}_k$ and the velocities $\vec{v}_k$ at the corresponding time t, leading to

$$f(\vec{x}, \vec{v}, t) = \sum_{k=1}^{N} w_k \delta(\vec{x} - \vec{x}_k(t))\delta(\vec{v} - \vec{v}_k(t)). \qquad (2)$$

Additionally, the particle weighting factor w_k is introduced, which allows the handling of large particle numbers with a lower number of simulation particles. A typical time step of PICLas is shown in Fig. 2. Due to the operator splitting approach, a consecutively execution of all solvers (PIC, DSMC, etc.) is possible.

The DSMC method, which was first introduced by Bird [1], performs collisions among freely moving particles and between particles and boundaries of the computational domain. Each collision includes an energy and momentum exchange and optionally a relaxation process of internal degrees of freedom as well as chemical reactions. A typical time step for DSMC is depicted in Fig. 3.

In the pairing process, two particles are chosen for a possible collision. The pairing itself can be done by different

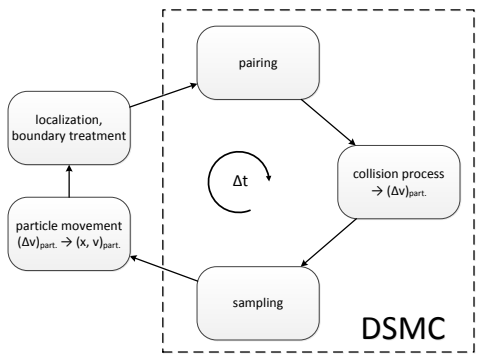

Figure 3: Typical time step of the DSMC method.

ways, as long as the distance between the chosen particles is smaller than the mean free path of the gas, e.g. by mesh adaptation [1]. In PICLas, particle pairing is done on the basis of searching the nearest neighbor in each computational cell. Additionally, this pairing method is combined with an octree scheme in order to reduce the computational costs of searching for the nearest neighbor [20].

The collision process can lead to the relaxation of inner degrees of freedom as well as to chemical reactions. PICLas enables the handling of rotational energy modeled as a rigid rotor in a continuous manner. The vibrational energy is treated using the quantized harmonic oscillator model. For the electronic excitation energy, the exact quantized energies and degeneracies are read in as a database for each species. This is an important advantage of the DSMC method compared to classic CFD models for the radiation coupling. In the DSMC model, the inner energies, which are the key source for the radiation process, are not restricted to a Boltzmann distribution. Instead, each particle carries quantized energies for the vibrational and electronic excited states. This allows for a much more detailed investigation of non-equilibrium effects in radiation processes. Experimental studies have shown that these non-equilibrium effects can be crucial for the correct prediction of radiation heat fluxes and interpretation of spectrometer measurements [13]. PICLas uses a Larsen-Borgnakke model described in Ref. [3] for the relaxation process. It is worth mentioning that polyatomic species (such as CO_2 and CH_4) are modeled in PICLas as well [21]. In this case, each molecule possesses more than one vibrational quantum number according to the number of atoms in the molecule.

In addition to the relaxation of the inner degrees of freedom, collisions can lead to chemical reactions. Two approaches to model chemical reactions are implemented in PICLas, enabling ionization and charge exchange reactions in addition to the common chemical reactions, such as dissociation, recombination and exchange reactions. The first model is the standard DSMC chemistry model, based on the extended Arrhenius equation [1]. The reaction probability depends on the Arrhenius coefficients, which are typically determined by measurements under continuum conditions. Thus, the Arrhenius equation needs a macroscopic temperature value, which is not defined in a collision of two particles. Therefore, the microscopic collision energy has to be translated to a macroscopic temperature by making equilibrium assumptions. The second implemented model is the Quantum-Kinetic (Q-K) model proposed by Bird [2], which depends solely on statistical mechanics and offers a phenomenological approach. As a result, the Q-K model depends only on the collision energy and fundamental species data.

The last step in the DSMC method is the sampling of macroscopic values like density, bulk velocity or temperature that are of interest in most engineering problems rather than particle information like internal energies or microscopic particle motion. The calculation of these macroscopic values is done by evaluating moments of the particle distribution function. Nevertheless, the calculation of temperatures for the inner degrees of freedom and for translation leads to a loss of information about the distribution function itself. To capture non-equilibrium effects correctly, a more sophisticated approach for a coupling with a radiation solver, which will be investigated in future work, is to handle the sampled distribution function instead of sampled moments.

2.2. Line-By-Line Atomic Bound-Bound Radiation Modeling

Initially, it was planned to use PARADE (PlasmA RAdiation DatabasE) [24] to post-process the flow field data in terms of radiation calculation. PARADE is a line-by-line code to calculate radiative properties in terms of spectral emission and absorption coefficients. The development started in 1994 cooperatively by the Institute of Space Systems (IRS) and Fluid Gravity Engineering (FGE), supported by the European Space Agency (ESA). PARADE is a combination of an extensive database and various routines needed to process this data for a given thermodynamic condition. Its capabilities include the calculation of radiation for numerous atomic and molecular species, the ability to account for different radiation mechanisms (bound-bound, bound-free, and free-free), as well as the consideration for various line broadening processes.

Concerning the purpose of a coupling with a DSMC module, however, there are several difficulties using PARADE. The temperature input is limited to one translational and one electronic excitation temperature, which are used for all species. Also, the outdated code structure makes parallelization very difficult and data transfer from PICLas to PARADE and back in a high-performance computing context is not possible without extensive code changes. Due to the cost of effort of a long-term code development, the decision was therefore made to implement the physics of PARADE into a new code structure within the PICLas framework. The extensive database of PARADE shall be maintained and the use of all predefined characteristics for energy levels and transition lines shall be enabled. The following section gives an overview of the implemented bound-bound radiation.

2.2.1. Atoms

Radiation modeling of bound-bound transitions requires at least knowledge about the spectral position of a transition line, its intensity, and its shape. In this section, a line-by-line concept of atomic bound-bound radiation is presented.

Line position. All atomic bound-bound radiation results from pure electronic transitions. It can be illustrated by Bohr's atomic model, which depicts the principles of radiation from electronically excited states despite

its generally limited validity. An excited electron corresponds to a higher orbit and has a limited residence time in this excited state. The electron drops back to an energetically lower level by emitting a photon if the energy is not transmitted to another particle non-radiatively by collision. The energy of the photon is described exactly by the difference between the energies of the two electronic states, leading to a defined frequency ν.

$$E_{photon} = h\nu = E'_{el} - E''_{el} \tag{3}$$

The different energy levels and, therefore, the spectrum are characteristic for each species.

Line intensity. The line intensity for each transition line relates to the emission coefficient ε for a specific line

$$\varepsilon = n' \frac{A_{'\rightarrow''} h\nu}{4\pi}, \tag{4}$$

with the upper state density n', the Einstein coefficient for spontaneous emission $A_{'\rightarrow''}$, the Planck constant h, and the frequency of the emitted light ν. Therefore, the line intensity depends on the transition probability in terms of the Einstein coefficient for spontaneous emission

$$A_{'\rightarrow''} = \frac{16\pi^3\nu^3}{3\varepsilon_0 hc^3} |\langle\psi'|\mu(r)|\psi''\rangle|^2, \tag{5}$$

where ε_0 is the vacuum permittivity and the primed and double primed values denote upper and lower state, respectively. The transition moment $|\langle\psi'|\mu(r)|\psi''\rangle|^2$ is defined by the squared overlap integral of the wave functions of involved upper and lower states and the corresponding dipole moment $\mu(r)$.

Line broadening. Owing to the finite lifetime of the atomic states, the transition line is not infinitely sharp. Also, the plasma perturbs the eigenstates of emitting atoms and ions so that the transitions are both broadened and shifted from their unperturbed values [5]. All broadening mechanisms can be described with Lorentzian or Gaussian profile functions and their corresponding full widths at half maximum (FWHM). The combined effect of two independent line broadening mechanisms is given by the convolution integral of the two profile functions, in this specific case resulting in a Voigt profile. Its width is a rather complicated function of the widths of the Lorentzian and Gaussian lines. Attempts have been made to find simplified relationships. In this work, the approach of Olivero & Longbothum [17] is used, which describes the Voigt-width with a maximum inaccuracy of 0.02%. For atomic radiation, Lorentzian profile widths are calculated for natural broadening, Stark broadening, Van der Waals broadening, Lorentz broadening, and resonance broadening, as already implemented in PARADE [24]. The total Lorentzian broadening is obtained by adding up the single components. The broadening due to the thermal translational motion of the atoms (Doppler-effect), the so called Doppler broadening, results in a Gaussian profile function and is also considered in PARADE [24].

Results. Based on the information about the position, the intensity, and the shape of the transition lines, spectral emission coefficients are calculated. Energy levels and Einstein coefficients, which are necessary for the calculation, are taken from NIST [11] and Wiese et al. [25] and are already implemented in the used database of PARADE. A comparison of results from PARADE with results from the developed radiation solver in the PICLas framework is given in Fig. 4. Figure 4(a) shows the emission spectrum of atomic nitrogen (N_I) and atomic oxygen (O_I) at translational temperatures of 2000 K, electronic excitation temperatures of 10 000 K and number densities of $2.46 \cdot 10^{21}\,\mathrm{cm}^{-3}$. Figure 4(b) shows the atomic oxygen triplet at 777 nm with a finer discretization at the same conditions. An excellent agreement can be stated.

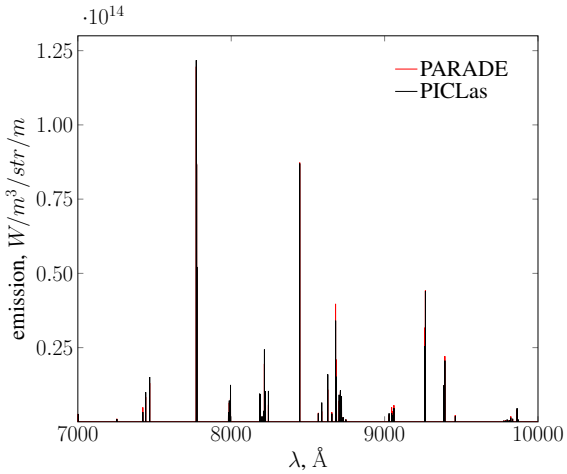

(a) Infrared spectrum

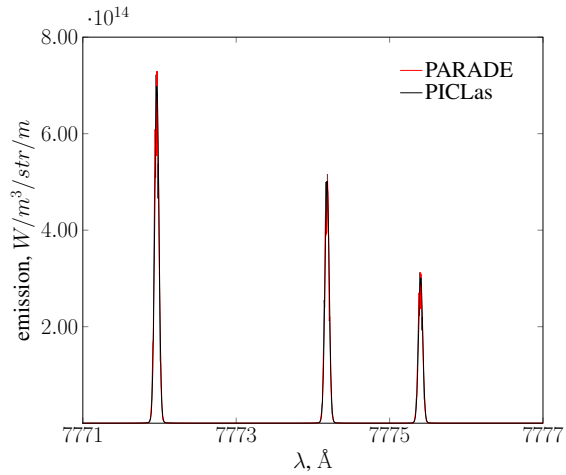

(b) Fine structure

Figure 4: Comparison of atomic bound-bound radiation in a single cell of calculations with PARADE and the developed radiation solver.

2.2.2. Molecules

The modeling of molecular radiation again requires at least knowledge about the line position, the line intensity, and the line shape. In this section, a line-by-line concept of molecular bound-bound radiation for diatomic molecules is presented.

Line position. Compared to atoms, molecules do not produce specific transition lines but complete bands due to the ability to store energy in additional inner degrees of freedom (vibration and rotation). The energy difference of a rotationally, vibrationally and electronically excited molecule is given by

$$\Delta E = h\nu = \Delta E_{el} + \Delta E_{vib} + \Delta E_{rot}. \tag{6}$$

For further calculation, it has been proven beneficial to use the energy normalized by the product hc, since a direct conversion into wavenumbers $\bar{\nu}$ is possible:

$$\bar{\nu} = T_{e'} - T_{e''} + G_{e',v'} - G_{e'',v''} + F_{e',v',J'} - F_{e'',v'',J''} \tag{7}$$

The upper state is described by the quantum numbers e', v', and J' for the electronic excitation ($T_{e'}$), the vibrational excitation ($G_{e',v'}$), and the rotational excitation ($F_{e',v',J'}$). The lower state is indicated by the superscript $''$. The vibrational energy of an anharmonic oscillator is described by

$$\begin{aligned} G_v = & \underbrace{\omega_e \left(v + \frac{1}{2}\right)}_{\text{I}} \underbrace{-\omega_e x_e \left(v + \frac{1}{2}\right)^2}_{} \ldots \\ & \underbrace{\ldots + \omega_e y_e \left(v + \frac{1}{2}\right)^3 - \omega_e z_e \left(v + \frac{1}{2}\right)^4 + \ldots}_{\text{II}}, \end{aligned} \tag{8}$$

with the vibrational quantum number v and the vibrational constants ω_e, $\omega_e x_e$, $\omega_e y_e$, and $\omega_e z_e$, which result from the Dunham expansion [6]. A harmonic oscillator is assumed (I), which needs to be corrected by higher order terms (II), since Coulomb repulsion occurs if the nuclei are closer, and dissociation if the distance between the nuclei is enlarged. The rotational energy is defined by

$$F_{v,J} = \underbrace{B_v J (J+1)}_{\text{I}} \underbrace{-D_v J^2 (J+1)^2 + \ldots}_{\text{II}} \tag{9}$$

with the vibrational coupling constants

$$B_v = B_e - \alpha_e \left(v + \frac{1}{2}\right) + \gamma_e \left(v + \frac{1}{2}\right)^2, \tag{10}$$

$$D_v = D_e - \beta_e \left(v + \frac{1}{2}\right). \tag{11}$$

The spectroscopic constants B_e, D_e, α_e, β_e, and γ_e result again from the Dunham expansion [6]. The model of a rigid rotor (I) needs to be corrected since the distance between the nuclei changes with an increasing rotational quantum number J, thus the centrifugal distortion constant D_e is implemented (II).

Line intensity. In order to obtain an emission spectrum, the intensities of the single transition lines need to be determined. Basically, the intensity of a single emission line of a molecule results from the transition probability due to quantum mechanical considerations and due to the upper state density

$$\varepsilon = \frac{16\pi^3 c \bar{\nu}^4}{3} n' \left(R_e \left(\bar{r}_{\nu',\nu''}\right)\right)^2 q_{\nu',\nu''} \frac{S^{J'\Lambda'}_{J''\Lambda''}}{2J'+1}. \tag{12}$$

In general, the upper state density n' is determined by distribution functions. In a first approach, equilibrium assumptions are made and Boltzmann distributions are used. The transition probability is significantly influenced by the Franck-Condon principle and the Franck-Condon factor $q_{\nu',\nu''}$, which are measures for the intensity of a vibrational band. Another measure for the intensity of a vibrational band is the transition dipole moment $R_e\left(\bar{r}_{\nu',\nu''}\right)$. The Hönl-London factor $S^{J'\Lambda'}_{J''\Lambda''}$, which depends on the rotational quantum number J, controls how the $(2J+1)$ allowed states are distributed among the branches and, therefore, is a measure fo the intensity of the rotational bands. The equations for calculating the Hönl-London factors $S^{J'\Lambda'}_{J''\Lambda''}$ can be taken from Herzberg & Huber [7].

Line broadening. The line shape is approximated by Voigt profiles, which are the convolution of Lorentzian and Gaussian profile functions. Different broadening mechanism are used analogously to the atomic bound-bound radiation. Lorentzian profile widths values are calculated for natural broadening, pressure broadening, and a Stark contribution. Additionally, the Doppler broadening with a Gaussian profile function is considered, both according to the equations in PARADE [24].

Results. Based on the calculated line position, line intensity, and line shape, spectral emission coefficients are calculated. Energy levels and transition probabilities are taken from Laux [12] and are already implemented in the PARADE database. Figure 5 shows a comparison of three different radiating systems of molecular nitrogen, the Birge-Hopfield band in Fig. 5(a), the 1st Positive system in Fig. 5(b), and the 2nd Positive system in Fig. 5(c) at an equilibrium temperature of 10 351 K and a density of $3.38 \cdot 10^{21}\,\mathrm{cm}^{-3}$. An excellent agreement can be stated for all transition bands.

2.3. Radiative Transfer Solver

After determining the emission coefficient per unit wavelength ε_λ and the net absorption coefficient κ_λ in each cell using the radiation solver as described above, the next step is the calculation of radiative energy transfer within the simulation domain. For this purpose, the change of the radiation intensity in an arbitrary direction due to emission and absorption of the surrounding gas in the

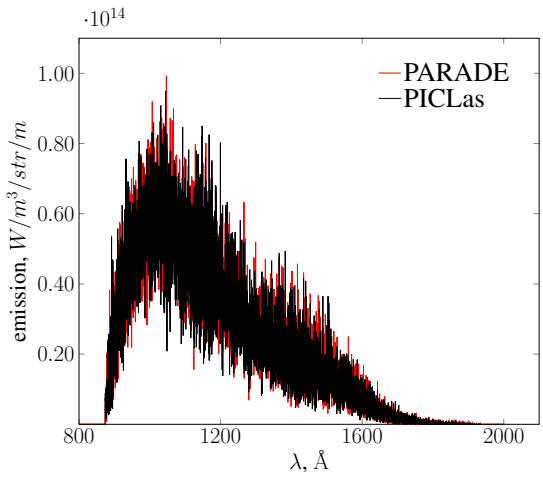

(a) N_2 Birge-Hopfield $\left(B^1\Pi \rightarrow X^1\Sigma\right)$

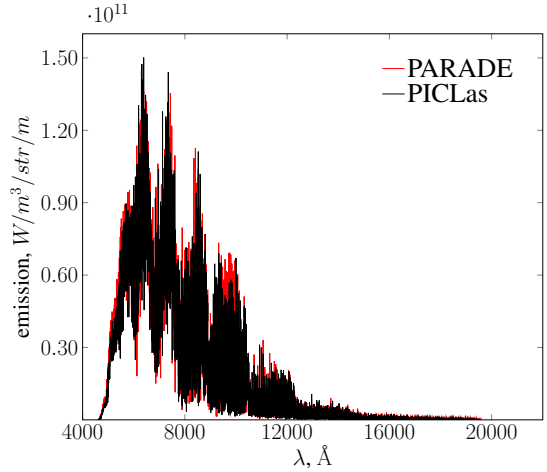

(b) N_2 1st Positive $\left(B^3\Pi \rightarrow A^3\Sigma\right)$

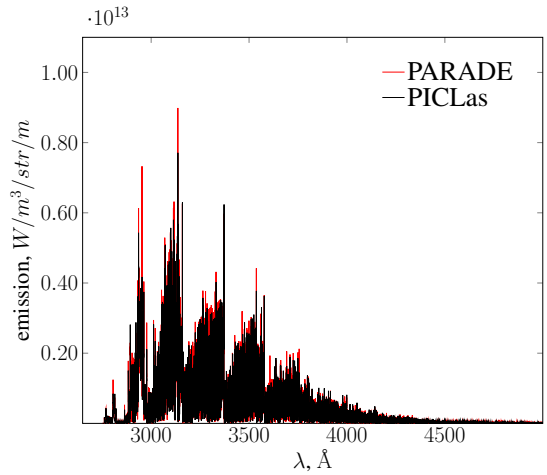

(c) N_2 2nd Positive $\left(C^3\Pi \rightarrow B^3\Pi\right)$

Figure 5: Comparison of molecular bound-bound radiation in a single cell of calculations with PARADE and the developed radiation solver.

simulation domain is investigated. This process is described by the radiative transfer equation (RTE), which is given by

$$\frac{dI_\lambda\left(x\right)}{ds} = \varepsilon_\lambda\left(x\right) - \kappa_\lambda\left(x\right) I_\lambda\left(x\right). \tag{13}$$

Here, I denotes the spectral radiation intensity depending on the wavelength λ. Furthermore, s and x are the measure of distance and the coordinate, respectively; both along the considered line of sight. Scattering effects within the gas are neglected and only the steady solution is considered due to the involved time scales.

Another quantity often used to describe the radiative transfer process is the heat flux q,

$$q = \int_0^\infty \int_{4\pi} I \, d\omega d\lambda, \tag{14}$$

or alternatively the divergence of the heat flux

$$\nabla \cdot q = \nabla \cdot \int_0^\infty \int_{4\pi} I \, d\omega d\lambda = \int_0^\infty \int_{4\pi} \frac{dI}{ds} \, d\omega d\lambda. \tag{15}$$

Since an analytical solution for the RTE exists only for simple cases, the RTE usually has to be solved by means of approximate models for radiative transfer. For this, different algorithms with different levels of accuracy and different computational effort are available. The main problem of solving the RTE equation using a classical numerical method, e.g. the finite element method, is the huge number of wavelengths λ for which the equation needs to be solved.

2.3.1. Monte Carlo method

An established method to solve the RTE is the Monte Carlo method [8, 14], which is distinguished by a high accuracy even for geometrically complex problems as well as a high flexibility to spectral and spatial resolution with the downside of high computational costs and statistical fluctuations, due to the use of random numbers. Its main idea is to trace a certain number of photon bundles with a fixed amount of the overall energy through the simulation domain, interacting with the surrounding gas by absorption. The initial properties of a photon bundle are the position, the wavelength, and the direction.

Number of photon bundles. The number of emitted photon bundles per cell are determined with two different methods. In the first method, each photon bundle carries the same amount of energy. A fixed number of photon bundles is created for the whole domain. The number of photon bundles n_i per cell i is then defined by

$$n_i = \frac{Q_i}{Q_{tot}} \cdot n_{tot}. \tag{16}$$

Here, n_{tot} is the fixed total number of photon bundles, Q_{tot} and Q_i are the total emitted radiation and the emitted radiation per cell, respectively:

$$Q_i = 4\pi \int_{V_i} \int_{\lambda=0}^{\infty} \varepsilon_\lambda \, d\lambda dV \tag{17}$$

$$Q_{tot} = \sum_{N_{cell}} Q_i. \tag{18}$$

Therefore, each photon bundle carries an energy portion of $\Delta Q = Q_{tot}/n_{tot}$.

In the second method, an equal number of photon bundles is emitted from each cell

$$n_{cell} = \frac{n_{tot}}{N_{cell}}. \tag{19}$$

Therefore, each photon bundle in a cell i carries an energy portion of $\Delta Q = Q_i/n_{cell}$ and, thus, the photon bundles from different cells carry different energy portions.

Initial position. The photon bundles are distributed randomly in the volume of their emitting cell.

Wavelength. The wavelength is determined randomly by comparing a random number ($0 \leq R_\lambda \leq 1$) with the distribution function P_λ for the radiation wavelength

$$P_\lambda = \frac{\int_0^\lambda \varepsilon_\lambda d\lambda^*}{\int_0^\infty \varepsilon_\lambda d\lambda} \tag{20}$$

in the corresponding cell. λ is taken as the wavelength for the photon bundle if $P_\lambda > R_\lambda$.

Direction. The directions of the photon bundles are determined with two different methods. In the first method, the normalized direction vectors $\mathbf{d}$ are generated by randomly distributing points on a unit sphere, using two random numbers R_1 and R_2 for each point:

$$\alpha_1 = 1 - (2R_1 - 1)^2, \quad \alpha_2 = \pi(2R_2 - 1) \tag{21}$$

$$\mathbf{d} = (\sin(\alpha_2)\sqrt{\alpha_1}, \cos(\alpha_2)\sqrt{\alpha_1}, 2R_1 - 1) \tag{22}$$

Since the Monte Carlo method has the disadvantage of statistical noise, especially for a low number of photon bundles, a second, different method is implemented. Here, the direction vectors with a vector norm of one are equally distributed over a unit sphere in a spiral configuration [10] to ensure a coverage of all spatial directions. An exemplary comparison for 200 photon bundles is shown in Fig. 6. In order to reduce computational costs, it is beneficial to use the same spiral in each cell and, therefore, the same number of photon bundles. To prevent unwanted preferential directions due to the deterministic methods, the spheres are rotated by randomly chosen, uniformly distributed angles.

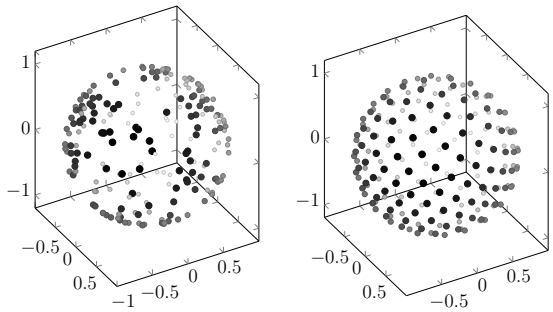

(a) Randomly distributed (b) Equally distributed

Figure 6: Variation of the direction distribution on the surface of a unit sphere for 200 photons.

Absorption. Using its assigned initial position and its direction, the optical path of each photon beam is calculated. Tracing of the bundle trajectories through the computational domain requires an efficient ray tracer, which is adopted from the particle tracking routines in PICLas [15]. For each photon bundle, the RTE is solved along the calculated optical path. Two different methods for the absorption are investigated, a statistical and a deterministic approach. Using the statistical approach, the total absorption along the optical path within a cell is calculated and compared to a random number to determine whether the photon bundle is absorbed or further considered. The condition for the absorption of the bundle in cell i is

$$-\log(R_a) < l^i \kappa_\lambda^i \tag{23}$$

with the traveled distance l^i in the cell, the local absorption coefficient κ_λ^i and a uniformly distributed random number R_a.

In contrast, the deterministic approach reduces the energy of the photon bundle in every grid cell until the energy reaches a minimum limit ε_Q and the photon bundle is absorbed. The new energy of a photon bundle after traveling through a cell i is given by

$$\Delta Q^{new} = \Delta Q e^{-l^i \kappa_\lambda^i}. \tag{24}$$

2.3.2. Infinite cylinder test case

To verify the numerical implementation, the radiative transfer is tested against the analytical solution of an infinitely long cylinder filled with a gas emitting black body radiation. Within the cylinder, the medium is assumed to be homogeneous with a constant temperature of $T = 10\,000\,\mathrm{K}$ and a constant absorption coefficient of $\kappa(r) = \kappa = 1\,\mathrm{m}^{-1}$. A cylinder with a radius of $R = 1\,\mathrm{m}$ and a length of $l = 100\,\mathrm{m}$ is used as computational domain. Two different mesh sizes, which are shown in Table 1, are used, one with 340 grid cells in the cross section (coarse mesh) and the other one with four times as many cells in the cross section (fine mesh), both with 400 cells in the length direction. An analytical solution for a one-dimensional radiative transfer of this test case is given e.g. by Kesten [9] and Sakai et al. [23].

Table 1: Mesh parameters for the calculated semi-infinite cylinder test case.

Mesh conditions		
Refinement	coarse	fine
Cross-section	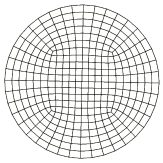	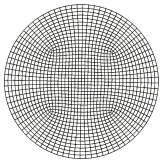
n_{cells}	340x400	1360x400
Length, m	100	
Radius, m	1	
T, K	10000	
κ, m^{-1}	1	

For a black body, the emission coefficient is given by

$$\varepsilon(\lambda) = I_p(\lambda, T), \tag{25}$$

where I_p is the Planck distribution

$$I_p(\lambda, T) = \frac{2hc^2}{\lambda^5} \frac{1}{e^{\frac{hc}{\lambda k_B T}} - 1}. \tag{26}$$

Here, h denotes the Planck constant, c the speed of light in vacuum, and k_B the Boltzmann constant.

The divergence of the heat flux for a constant black body radiation and a constant absorption coefficient are shown in Fig. 7. Both methods for the determination of the number of photon bundles per cell were investigated but showed only negligible differences due to locally equal temperatures and, therefore, equal emission. However, in a more anisotropic plasma, this needs to be tested again since larger deviations for the two approaches are expected. Figure 7a compares the two absorption models on the fine mesh for different numbers of photon bundles. The deterministic approach leads to better results and less fluctuations, therefore, this method is selected for further calculations. The two implemented direction distributions are compared in Figs. 7b and 7c for the coarse and the fine mesh, respectively. The approach with equally distributed directions shows more precise results for any number of photon bundles on both investigated meshes. Figure 7d shows that this is still the case for small numbers of photons and correspondingly increased statistical noise.

3. CONCLUSION

The radiative heat flux can be substantial during atmospheric entries with high velocities. While conventional CFD methods can generate a flow field solution, radiation

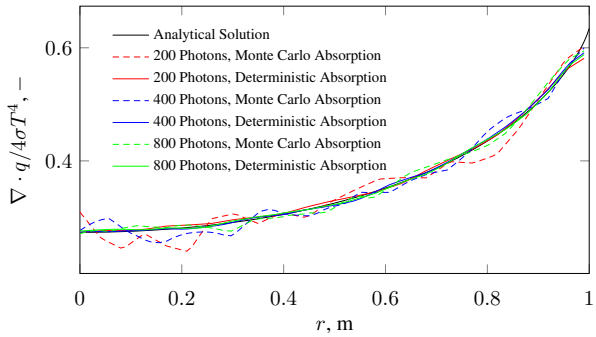

(a) Comparison of absorption models (fine mesh)

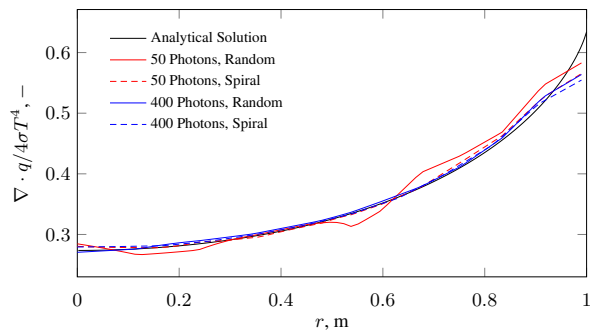

(b) Comparison of direction distribution methods (coarse mesh)

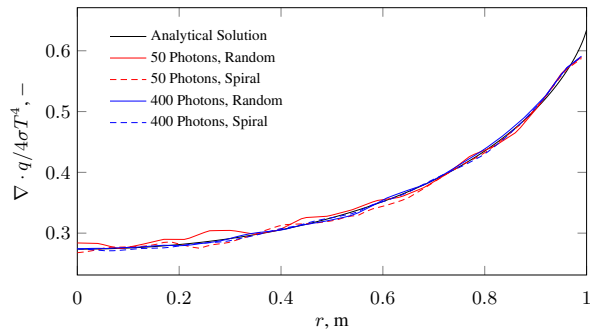

(c) Comparison of direction distribution methods (fine mesh)

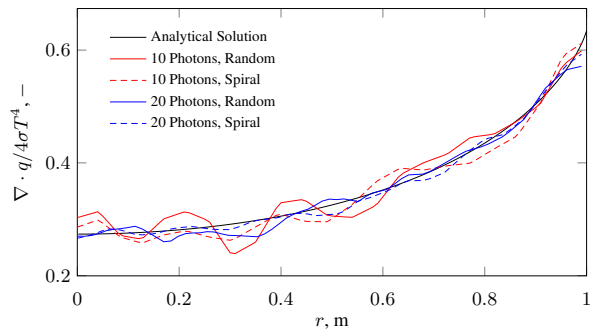

(d) Comparison of direction distribution methods for low photon numbers (fine mesh)

Figure 7: Divergence of the heat flux of black body radiation in a quasi-infinite cylinder.

transport solvers require more detailed information such as the distribution functions within different internal degrees of freedom. Particle methods such as the DSMC method can not only produce physically accurate results for non-equilibrium conditions but offer a detailed insight into a flow field. Consequently, the first steps toward coupling the DSMC method and a radiation solver were described. The radiation solver PARADE was found not to be suitable for such a coupling, therefore, a new, direct implementation of a radiation solver in the PICLas framework has been initiated. As a first step, bound-bound radiation for atoms and molecules has been realized. Results of cell-local computations were presented and compared to results of PARADE. An excellent agreement can be stated for both, atomic and molecular radiation. Exemplary simulations have been conducted on the basis of O, N, and three different bands of N_2. Furthermore, a concept for solving the radiative transfer equation using a Monte Carlo approach was presented. For a quasi-infinite cylinder with black body radiation, a classical and a noice-reducing approach with equally distributed directions of the photon bundles in each cell were compared, showing more precise results with the latter method. Additionally, a statistical and a deterministic method to handle the photon bundle energy in terms of absorption were investigated, with the deterministic method showing better results.

In future work, continuum radiation will be implemented into the radiation solver. Furthermore, the flow field solver, the radiation solver, and the radiation transfer solver will be coupled and applied to the calculation of a reentry case. For this, as a first step, the developed radiation solver will use temperatures and densities as input parameters as presented in this paper. Next, a more sophisticated approach could be to sample the distribution functions of each degree of freedom in each grid cell instead of sampling the moments of the distribution functions to evaluate macroscopic values.

ACKNOWLEDGMENTS

The authors gratefully acknowledge funding provided by Airbus Defence and Space, by ArianeGroup and by the Deutsche Forschungsgemeinschaft (DFG) within the project "Partikelverfahren mit Strahlungslöser zur Simulation hochenthalper Nichtgleichgewichts-Plasmen" (project number 393159129).

REFERENCES

[1] Bird, G. 1994, Molecular Gas Dynamics and the Direct Simulation of Gas Flows, 2nd edn. (New York: Oxford University Press)

[2] Bird, G. A. 2011, Physics of Fluids, 23

[3] Borgnakke, C. & Larsen, P. S. 1975, Journal of Computational Physics, 18, 405

[4] Boyd, I., Zhong, J., Levin, D., & Jenniskens, P. 2008, in 46th AIAA Aerospace Sciences Meeting and Exhibit, 7-10 January 2008, Reno, Nevada

[5] Cooper, J., Institute of Physics (London, E., & Britain), P. S. G. 1966, Plasma Spectroscopy (Institute of Physics and the Physical Society)

[6] Dunham, J. L. 1932, Phys. Rev., 41, 721

[7] Herzberg, G. & Huber, K. 1950, Molecular Spectra and Molecular Structure: Spectra of Diatomic Molecules (Van Nostrand)

[8] Howell, J. 1998, ASME Journal of Heat Transfer, 120(3), 547

[9] Kesten, A. S. 1968, Journal of Quantitative Spectroscopy and Radiative Transfer, 8, 419

[10] Kogan, J. 2017, Rose-Hulman Undergraduate Mathematics Journal, 18: Iss. 2, Art. 5

[11] Kramida, A., Yu. Ralchenko, Reader, J., & and NIST ASD Team. 2018, NIST Atomic Spectra Database (ver. 5.6.1), [Online]. Available: `https://physics.nist.gov/asd`. National Institute of Standards and Technology, Gaithersburg, MD.

[12] Laux, C. 1993, PhD thesis, Stanford University

[13] Macdonald, R. L., Munafò, A., Johnston, C. O., & Panesi, M. 2016, in 54th AIAA Aerospace Sciences Meeting

[14] Modest, M. 2003, Radiative Heat Transfer, 2nd edn., Academic Press (Academic Press)

[15] Munz, C.-D., Auweter-Kurtz, M., Fasoulas, S., et al. 2014, Comptes Rendus Mécanique, 342, 662

[16] Nizenkov, P. 2018, PhD thesis, Institute of Space Systems, University of Stuttgart

[17] Olivero, J. & Longbothum, R. 1977, Journal of Quantitative Spectroscopy and Radiative Transfer, 17, 233

[18] Ozawa, T. 2007, PhD thesis, Department of Aerospace Engineering, Pennsylvania State University, University Park, PA

[19] Ozawa, T., Wang, A., Levin, D., & Modest, M. 2008, in 40th Thermophysics Conference, 23-26 June 2008, Seattle, Washington

[20] Pfeiffer, M., Mirza, A., & Fasoulas, S. 2013, Journal of Computational Physics, 246, 28

[21] Pfeiffer, M., Nizenkov, P., Mirza, A., & Fasoulas, S. 2016, Physics of Fluids, 28, 027103

[22] Pfeiffer, M., Nizenkov, P., Mirza, A., & Fasoulas, S. 2016, in 7th International Workshop on Radiation of High Temperature Gases, 21-25 November, Stuttgart, Germany

[23] Sakai, T., K. Sawada, K., & Mitsuda, M. 2001, Journal of Thermophysics and Heat Transfer, 15, 176

[24] Smith, A., Wood, A., Dubois, J., Fertig, M., & Pfeiffer, B. Oct. 2006, Plasma Radiation Database PARADE V2.2 (Tech. Rep. TR28/96 Issue 3, Fluid Gravity Engnineering Ltd)

[25] Wiese, W., Smith, M., & Glennon, B. 1966, Atomic Transition Probabilities, Volume I Hydrogen Through Neon (NSRDS-NBS 4)